Journal of Catalysis **204,** 372–377 (2001)
doi:10.1006/jcat.2001.3371, available online at http://www.idealibrary.com on IDEAL®

Pd Interaction with Reduced Thin-Film Alumina: XPS and ISS Study

N. Tsud, K. Veltruska, and V. Matolin[1]

Department of Electronics and Vacuum Physics, Charles University, V Holešovičkách 2, 18000 Prague 8, Czech Republic

Received April 17, 2001; revised August 3, 2001; accepted August 4, 2001

X-ray photoelectron spectroscopy and ion-scattering spectroscopy (ISS) were used to investigate the interaction of palladium with reduced thin-film alumina. The substrate was prepared by Ar^+ ion bombardment thinning of the natural oxide layer on polycrystalline aluminum foil. It was found that the constitution of a surface equilibrium is determined by the energy of sputtering ions. Therefore, after the sputtering, the aluminum oxide surface is covered by more or less Al^0-rich overlayer. During the first stage of the Pd deposition, the I_{Al}/I_O ratio decreases because of Pd atom deposition onto the Al sites, keeping the anionic oxygen sites unaffected. With increasing Pd, the PdAl intermetallic compound is formed. The alloy forms three-dimensional clusters and a bare alumina surface appears, giving the ISS intensity ratio I_{Al}/I_O characteristic for γ-Al_2O_3. At a high amount of deposited Pd, the Pd bulk-like phase is formed, gradually burying the PdAl alloy clusters. To interpret catalytic behavior of Pd/Al_2O_3 systems, the presence of the PdAl alloy caused by strong metal–substrate interaction should be considered.

Key Words: **X-ray photoelectron spectroscopy (XPS); ion-scattering spectroscopy (ISS); PdAl alloy; alumina (Al_2O_3); metal–substrate interaction (MSI); bimetallic interaction.**

1. INTRODUCTION

The investigation of structure and properties of small metal particles represents an important field of research in heterogeneous catalysis. A catalytically active component such as a transition metal is dispersed over a suitable support such as alumina or silica. Due to the high metal dispersion, the so-called particle-size effect, originating in structural or electronic properties of metal clusters, as well as the metal–substrate interaction (MSI) can influence the catalytic properties significantly.

Because of its great importance, numerous studies have been devoted to this field. The results of model studies performed with well-defined particles deposited on well-ordered bulk or film oxide surfaces showed how powerful surface-sensitive techniques are for structure-dependent size-effect investigations (see, e.g., the excellent reviews (1–3)).

Metal–substrate interaction is one of the catalyst behaviors for which knowledge is still very limited with regard to the relationship between the catalytic activity of deposited metal clusters and the supporting chemical composition and structure. Most model studies have been carried out on flat aluminum oxides, such as bulk crystals and thin films. Single-crystal α-Al_2O_3 frequently has been used as model support because of its mechanical and thermal stability (4–6). A variety of thin oxide films supported on metal substrates have been used because of their compatibility with transmission electron and scanning tunneling microscopy and electron spectroscopic techniques (1, 7–11).

Properties of aluminum oxide film were investigated extensively in the past (12–14). It was pointed out that oxide film structure and surface stoichiometry depend strongly on the film preparation and cleaning procedure applied (3). Often, the oxide surface preparation introduces noncontrolled surface perturbations (15), which may create strong MSI states (i.e., cationic or anionic vacancies). These highly active sites of the metal–oxide interface region may be responsible for particular MSI effects occurring at the particle edge, i.e., at the metal–oxide boundary (16). In addition, the catalyst metal can form intermetallic compounds with the reduced support (e.g., Pd–Al (17, 18), Pd–Sn (19)) that exhibiting strong bimetallic interaction through the hybridization of the d and s states (20), leading to the formation of alloys with special catalytic properties (21).

The number of palladium–alumina MSI studies is relatively limited because aluminum oxide is generally considered to be an inert, nonreactive support. However, in the case of palladium–alumina, some reports show the existence of metal–support charge transfer, indicating the MSI effect (22–27). This behavior is given by the higher Pd–Al electronegativity difference compared with that for Pd–O, which induces a stronger metal-cation interaction. Therefore, while metals like Cr, Ni, and Cu are bonded to the oxygen sites, Pd forms bonds with the aluminum sites, causing stronger MSI in the case of the reduced alumina surface (23).

The aim of this work was to show that the Pd interaction with nonstoichiometric (metal-rich) alumina may be the origin of MSI effects such as the anomalous lowering of

[1] To whom correspondence should be addressed. Fax: 420 2 688 5095. E-mail: matolin@mbox.troja.mff.cuni.cz.

0021-9517/01 $35.00

CO desorption temperature with decreasing Pd particle size (11), which is characteristic for CO desorption from Pd–Al intermetallic compounds (18).

In this report we present the results of X-ray photoelectron spectroscopy (XPS) and ion-scattering spectroscopy (ISS) studies of Pd interaction with ultrathin nonstoichiometric films of alumina prepared by Ar^+ ion sputtering of native oxide layer formed on aluminum polycrystalline substrate. The significant effect of oxygen preferential sputtering leads to the preparation of an aluminum-rich oxide surface. The subsequent Pd deposition under ultrahigh vaccum (UHV) conditions is conducive to the formation of a Pd–Al bimetallic interfacial layer, which is followed by the formation of a metal-like Pd phase.

2. EXPERIMENTAL

The XPS and low-energy ISS measurements were carried out in the ion-pumped UHV chamber with a base pressure of 10^{-7} Pa. The system was equipped with a dual Al/Mg X-ray source, differentially pumped ion gun for sputtering and ion scattering, and multichannel hemispherical analyzer Omicron EA 125.

In this work the Mg$K\alpha$ line (1253.6 eV) was used for XPS measurements. The photoelectron analyzer was operated in the retarding-field mode with the pass energy of 20 eV. The sample surface was characterized by photoelectron peaks of Al 2p, Pd 3d, O 1s; Auger peaks of Al (KLL) and Pd (MNN); and the valence band (VB) spectrum. The accuracy of the measured binding energies was better than ± 0.1 eV.

Ultrathin Al_xO_y film was prepared by Ar^+ ion bombardment (0.5 (1.0) keV, 0.7 (1.9) $\mu A\,cm^{-2}$) of a natural oxide film on chemically cleaned polycrystalline Al foil (purity 99.999%). The cleanliness of the surface as well as the possible effect of preferential sputtering of oxide surface components, which may cause the changes in surface stoichiometry, was monitored by means of XPS and ISS analysis during the bombardment. ISS was carried out using He ions at primary energy of 2 keV. The thickness of the alumina layer (2.2 nm) was estimated by XPS from the Al_{ox}/Al_m ratio of the 2p peak intensity. Because the oxide film was very thin, the charging effect was absent during the spectroscopic studies.

The palladium was deposited on the thin aluminum oxide *in situ* at room temperature using the microelectron beam evaporation source (MEBES) (28), which allowed control of the evaporation rate by monitoring the Pd^+ ion current. We used a constant deposition rate of 1.5×10^{12} atoms s^{-1}, the value of which was determined from the XPS data. The XPS and ISS spectra were collected between particular depositions. The deposited layer morphology was investigated by analysis of the peak shape and background using QUASES software by Tougaard ApS. The principles of the method are explained in Ref. (29).

3. RESULTS AND DISCUSSION

3.1. Thin, Reduced Al_xO_y Oxide Film on Polycrystalline Al Foil

We started by preparing the metal-rich surface of thin alumina oxide layer by several doses of Ar^+ ion sputtering of the native oxide on the polycrystalline aluminum foil. We made a series of bombardments at different energies of incident ions: 0.5 and 1 keV. The native oxide layer thickness was estimated to be 5.6 nm from the ratio of the Al 2p XPS peak intensity corresponding to oxide and metal states. The ISS and XPS spectra were collected after each ion bombardment cycle, which allowed us to investigate the structure and surface stoichiometry of the oxide.

At the beginning we observed both metallic Al^0 and oxide Al^{3+} aluminum peaks at binding energies E_B of 72.9 and 75.9 eV, respectively (not shown). The energy difference between these two peaks was 3 eV and stayed constant during sputtering. The most distinct changes in XPS spectra were the decrease of the oxide and the increase of the metal component of the Al 2p peak. The Al^{3+}-to-Al^0 peak ratio decreased during the sputtering from 7.5 to 1.1, the final value before the deposition of palladium. The Auger parameter of aluminum, 1461.5 eV in oxide and 1466.2 eV in metal states, was found to be unchanged. That means that sputtering did not influence the stoichiometry of the inner part of the oxide layer. (The Auger parameter is a very sensitive probe of the physical and chemical environment of the analyzed atoms). The Auger parameter values were very close to values reported for γ-alumina (1461.6) and Al metal (1466.1) in (12), which confirmed that native oxide was composed of γ-alumina microcrystallites rather a being of amorphous phase (3). Valence-band changes resulted in the appearance of a plateau near the Fermi level that corresponded to the delocalized s,p states of free Al on the surface (Fig. 1).

Ion-scattering spectroscopy is a surface analytical technique that is sensitive to the very first atomic layer of the surface. The measured spectrum gives the intensity distribution of the scattered He ions versus their kinetic energy, which is directly related to the mass of the target atoms. Figure 2 shows the typical ISS spectra of the Al_xO_y/Al surface after bombardment. The integral intensity of ISS peaks was calculated after subtraction of the linear background. Since the neutralization terms for Al and O in alumina are unknown, it is impossible to determine exactly the stoichiometry of this layer without using a standard. However, the aluminum/oxygen scattering ion intensity ratio I_{Al}/I_O is directly proportional to the real surface stoichiometry. The values of the I_{Al}/I_O ISS intensity ratio during sputtering cycles are shown in Fig. 3. It can be seen that the I_{Al}/I_O ratio increases during sputtering and its value depends considerably on the energy of sputtering ions. It remains constant, close to 2, for ion energy of 0.5 keV, increases up to 8.8 for

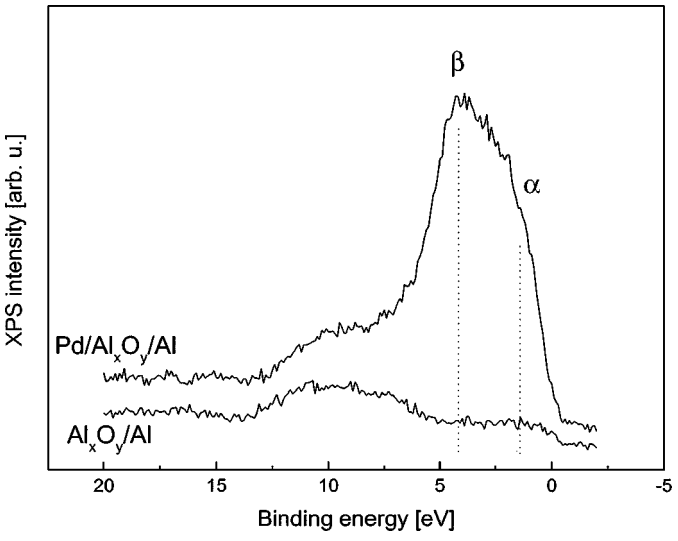

FIG. 1. Valence-band XPS spectra of bombarded alumina thin film on the polycrystalline aluminum before and after 30-min Pd deposition.

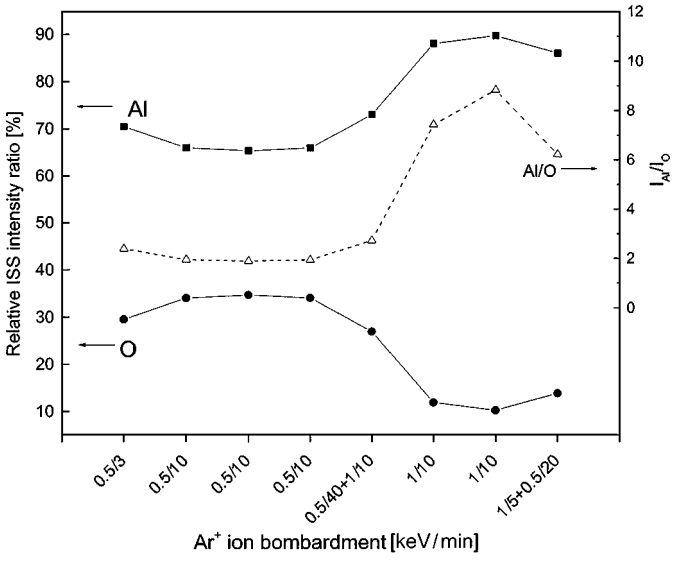

FIG. 3. The changes of the ISS peak intensities (Al and O) and the values of the I_{Al}/I_O intensity ratio during sputtering cycles.

1 keV, and reaches 6.2 after heating (10 min, 570 K) and final sputtering (0.5 keV, 20 min). This behavior can be explained by a preferential sputtering of oxygen from the surface that leads to the constitution of a new surface equilibrium determined by the energy of the incident ions. The left ordinate axis of Fig. 3 represents the composition of the surface, i.e., the ISS peak intensity for particular elements (Al or O) relative to the sum of the intensities of both components in percent. The I_{Al}/I_O intensities can be fitted with the function $K\theta_{Al}/(1-\theta_{Al})$, where θ_{Al} stands for the Al coverage, $(1-\theta_{Al})$ for the oxygen coverage, and K for a fitting parameter dependent on the neutralization of He^+ ions scattered by different surface atoms. Using the value of the ISS I_{Al}/I_O intensity ratio of 0.5, determined for the (0001)α-Al_2O_3 surface with known relative Al/O atomic coverage of 0.33 (30), we obtain the fitting parameter $K = 1.3$. Then the initial and final surface compositions of the oxide layer correspond to the aluminum/oxygen relative coverage $\theta_{Al} = 0.63$ and 0.82, respectively.

The results presented clearly show that the oxide surface is very sensitive to the energy of sputtering ions. Therefore, the surface with different stoichiometry can be prepared by changing the ion energy. Comparing the XPS and ISS results, we determined that the thin alumina layer of thickness ~2.2 nm covered by an Al-rich overlayer was prepared after using the bombardment procedure.

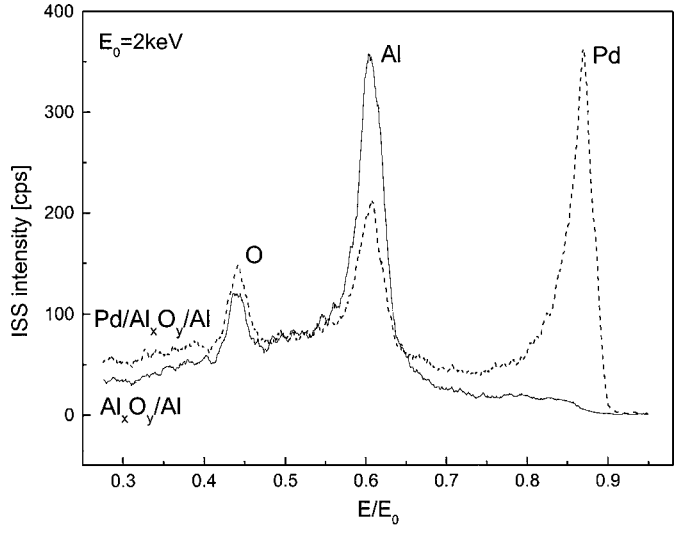

FIG. 2. ISS spectra of the Al_xO_y/Al surface before and after final Pd deposition.

3.2. Pd Deposition

The Pd layers were deposited at room temperature stepwise on the thin oxide layer described above. The Pd flux was kept constant during the deposition.

Figure 2 shows the ISS spectra obtained after 30 min of Pd deposition, corresponding to the equivalent thickness of 3 monolayers (ML). The ISS O and Al peaks are still clearly visible, indicating that the oxide surface is not completely covered by Pd (island growth mode).

The variations in Pd, Al, and O peak intensity during the deposition are shown in Fig. 4. As low-energy ISS is an extremely surface-sensitive technique, the component signals are indicative of the oxide surface composition changes given by Pd deposition. We have plotted the relative ISS signal intensities $I^{rel}_{Pd,Al,O} = 100\ I_{Pd,Al,O}/(I_{Al} + I_{Pd} + I_O)$ as a function of deposition time in Fig. 4. It can be seen that while the relative Pd signal is continuously growing and

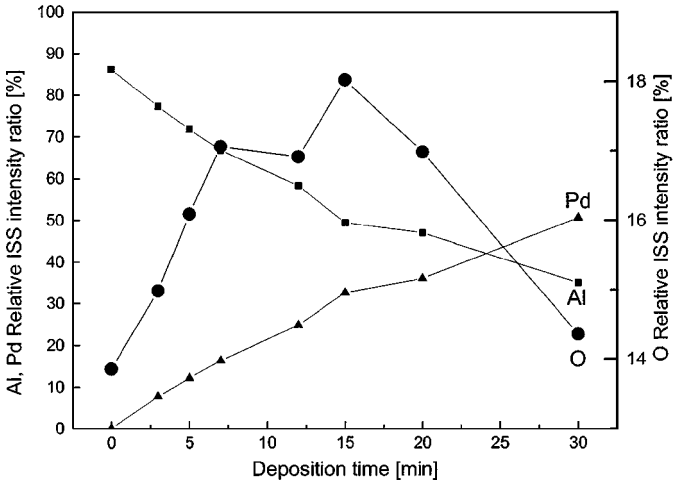

FIG. 4. The ISS intensity variations of Pd, Al, and O peaks during the Pd deposition.

Al signal falling, the oxygen relative intensity varies from an initial value of 13.8% to the final value of 14.4% via maximum of 18% after 15 min of deposition. This rather surprising behavior represents one of the key results of this study. This means that the relative surface concentration of oxygen sites not only remains unaffected by the Pd deposition but is increasing in certain limits. After the deposition, the ISS intensity ratio I_{Al}/I_O reaches the value of 2.4 very close to that of the nonsputtered alumina layer surface (see Fig. 3). Because the UHV conditions prevent surface reoxidation, this behavior can be explained by the appearance of a bare alumina surface. We conclude that Pd atoms form, with surface aluminum atoms, a buried layer of a PdAl intermetallic compound of three-dimensional (3-D) clusters. The hypothesis of 3-D clusters seems more probable because of the continuous increase in Pd ISS signal during the deposition. This also is supported by the fact that PdAl alloy is characterized by a high cohesion energy and melts at 100 K higher than does pure Pd (31). The high surface free energy of the formed alloy leads consequently to the formation of 3-D clusters. It should be noted that the same behavior has been observed in the case of Pd deposition on nonstoichiometric tin oxide (19).

Further information about Pd island formation on the bombarded surface of Al_2O_3/Al substrate was obtained from the XPS investigation. The binding-energy difference $E_B(Al_{ox}\,2p) - E_B(Al_m\,2p)$ obtained from XPS core level peaks is shown in Fig. 5. From the inset it can be seen that the oxide aluminum peak is shifted toward lower binding energy during deposition. The explanation for this behavior can be found by considering the following phenomena determining the electronic structure of thin nonstoichiometric oxide films: The relative concentration of aluminum on the sputtered layer of aluminum, determined from the ISS measurements, is approximately 0.8, showing the aluminum-rich surface with Al_4O surface stoichiometry. (It should be noted that for polycrystalline γ-Al_2O_3 prepared by thermal heating, as well as for the nonbombarded natural oxide layer, we obtained approximately Al_3O_2 stoichiometry.) The high concentration of anionic vacancies in the surface region leads to the reduction of the oxide gap width and to the appearance of gap states, with density corresponding to the degree of oxide reduction (32). In addition, the formation of a metal–oxide interface creates new, so-called metal-induced gap states (33). The creation of these high-lying states populates lower lying surface states, which is followed by charge transfer to unoccupied metallic states of Pd until thermodynamic equilibrium is achieved. The established electric field between metal and oxide-depleted layer may be responsible for the band bending and consequently for the decrease of the Al 2p binding energy of electrons emitted from the positively charged layer of oxide. On the other hand, some modification of the screening potential due to the Pd deposition on the alumina surface, i.e., a variation of the extra-atomic relaxation energy, cannot be excluded.

The variation of the Pd 3d photoelectron peaks versus deposition time is shown in Fig. 6. We can see that at the beginning the Pd layer growth is characterized by a Pd $3d_{3/2}$ peak at constant $E_B = 337.4$ eV, labeled β. Longer deposition times result in the appearance of another well-resolved Pd $3d_{5/2}$ peak at lower binding energy α, which shifts continuously to lower E_B with increasing coverage, as can be seen in Fig. 7. The position, shape, and width of the component β coincide with the corresponding ones of the alloyed Pd and are in good agreement with previously published XPS characteristics spectra for PdAl alloy (34, 35). On the other

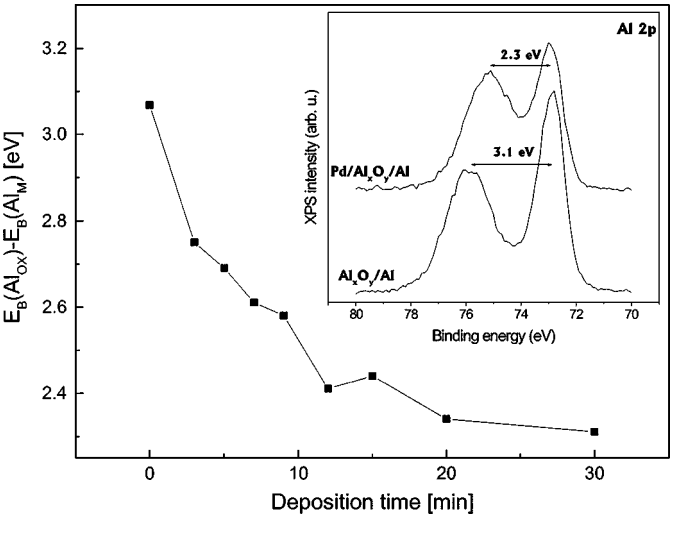

FIG. 5. The binding energy difference $E_B(Al_{ox}\,2p) - E_B(Al_m\,2p)$ obtained from XPS core-level peaks in dependence on increasing amount of deposited Pd. The inset presents the Al 2p peaks corresponding to the clear substrate and to that one after final deposition.

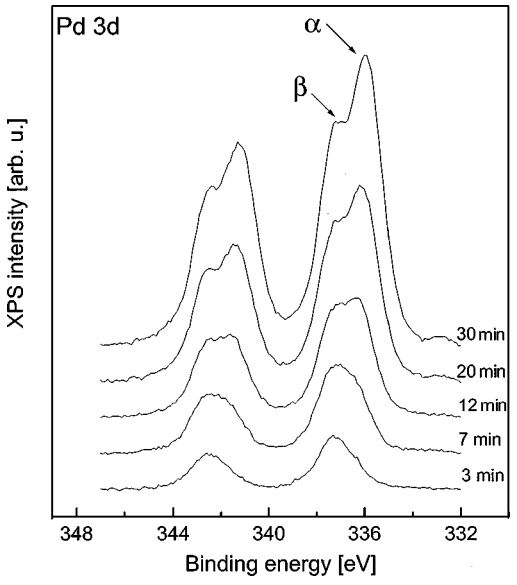

FIG. 6. The evolution of the Pd 3d doublet versus deposition time.

hand, an E_B decrease of the peak α toward Pd bulk value is typical for Pd cluster formation on the oxide surface (27). Thus, the measured Pd 3d intensity results from the mixture of two peaks, one of PdAl alloy at constant E_B (337.4 eV) and the other at size-dependent E_B for Pd particles.

The valence-band spectrum after final deposition is presented in Fig. 1, in which a combination of two other effects mentioned earlier also can be seen. The first is the creation of a PdAl alloy with the Pd 4d-centroid at 4.8 eV due to the strong hybridization of the Pd-d and Al-s states; the second is the formation of the Pd bulk-like d-band close to the zero E_B, which overlaps the alumina-valence band. Nevertheless, the opposite tendency in the intensity of these two components can be seen: the peak β near 5 eV remains higher than α. This behavior can be explained by the deeper information depth in the valence-band photoelectrons compared with the core level ones. The PdAl alloy clusters that are formed at the early stage of growth are gradually covered by the Pd overlayer, which attenuates the signal issued from the inner cluster in the case of surface-sensitive analysis. This explanation fits well with the ISS results. The I_{Al}/I_O ISS intensity ratio after final deposition corresponds to the nonbombarded alumina, indicating that the weakly bonded aluminum atoms move to buried PdAl clusters and do not contribute to the Al ISS signal.

XPS Pd background analysis shows a mode of growth similar to that of γ-alumina (27) which is characterized by the formation of flat islands with an average height of 1.2 nm.

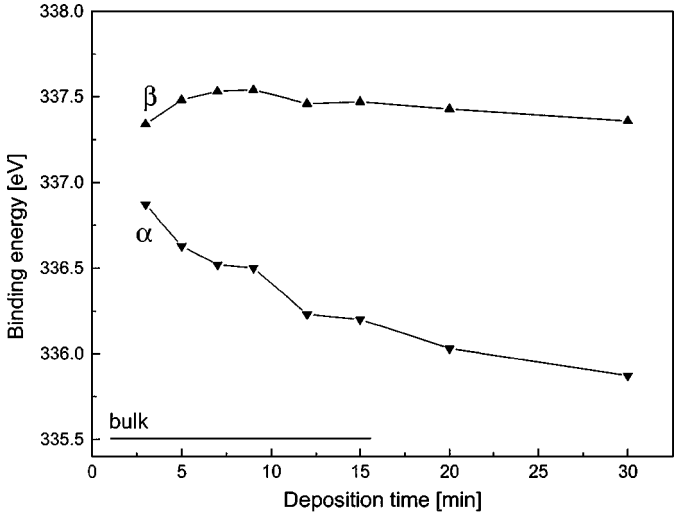

FIG. 7. The binding-energy variations of two components of the Pd $3d_{5/2}$ peak (shown in Fig. 6) during the deposition of Pd.

4. CONCLUSION

The increase in ISS intensity ratio I_{Al}/I_O during argon sputtering shows that oxygen is preferentially removed from the surface by argon bombardment. The surface equilibrium stoichiometry depends on the energy of the incident ions. Therefore, after the sputtering the aluminum oxide surface is covered by an Al^0-rich overlayer.

During the first stage of Pd deposition, the I_{Al}/I_O ratio decreases because of Pd atom deposition onto the Al sites, which keeps the anionic oxygen sites unaffected. With increasing Pd, the PdAl intermetallic compound is formed. The alloy forms 3-D clusters, and a bare alumina surface appears, giving the ISS intensity ratio I_{Al}/I_O characteristic for bare γ-Al_2O_3. At a higher amount of deposited Pd, the Pd bulk-like phase is formed, gradually burying the PdAl alloy clusters.

The observed formation of PdAl alloy can explain the appearance of a low-temperature desorption peak at 350 K in CO thermodesorption spectra from γ-Al_2O_3 and reduced α-Al_2O_3–supported small Pd particles (11, 6, 19), which corresponds to the CO-desorption temperature from bulk PdAl alloy (21). We propose that Pd–Al alloying on nonstoichiometric aluminum oxide surfaces should be taken into account in studies of reactivity of Pd on technological alumina powders.

ACKNOWLEDGMENT

This work was supported by the Czech Grant Agency under Grant 202/99/1714.

REFERENCES

1. Baumer, M., and Freund, H.-J., *Prog. Surf. Sci.* **61**, 127 (1999).
2. Henry, C. R., Chapon, C., Giorgio, S., and Goyenex, C., *in* "Chemisorption and Reactivity on Supported Clusters and Thin Films" (R. M. Lambert and G. Pacchioni, Eds.), NATO ASI Series E, Vol. 331, p. 117. Kluwer Academic, Dordrecht, Netherlands, 1997.

3. Gunter, P. L. J., Niemantsverdreit, J. W., Riberio, F. H., and Somorjai, G. A., *Catal. Rev. Sci. Eng.* **39**, 77 (1997).
4. Rumpf, F., Poppa, H., and Boudart, M., *Langmuir* **4**, 115 (1988).
5. Stara, I., and Matolin, V., *Surf. Rev. Lett.* **4**, 1353 (1997).
6. Jungwirthova, I., Stara, I., and Matolin, V., *Surf. Sci.* **377–399**, 644 (1997).
7. Goodmann, D. V., *Surf. Rev. Lett.* **2**, 9 (1995).
8. Goodmann, D. V., *Surf. Sci.* **299–300**, 837 (1994).
9. Bäumer, M., Frank, M., Heemeier, M., Kühnemuth, R., Stempel, S., and Freund, H.-J., *Surf. Sci.* **454–456**, 957 (2000).
10. Gillet, M. F., and Channakhone, S., *J. Catal.* **97**, 427 (1986).
11. Stara, I., and Matolin, V., *Surf. Sci.* **313**, 99 (1994).
12. Frederick, B. G., Apai, G., and Rhodin, T. N., *Surf. Sci.* **244**, 67 (1991).
13. Rhodin, T. N., Frederick, B. G., and Apai, G., *Surf. Sci.* **287 & 288**, 638 (1993).
14. Libuda, J., Winkelmann, F., Bäumer, M., Freund, H.-J., Bertrams, Th., Neddermeyer, H., and Müller, K., *Surf. Sci.* **318**, 61 (1994).
15. Stara, I., Zeze, D., Matolin, V., Pavluch, J., and Gruzza, B., *Appl. Surf. Sci.* **115**, 46 (1997).
16. Boffa, A., Lin, C., Bell, A. T., and Somorjai, G. A., *J. Catal.* **149**, 149 (1994).
17. Juszczyk, W., Lomot, D., Karpinski, Z., and Pielaszek, J., *Catal. Lett.* **31**, 37 (1995).
18. Matolín, V., Stará, I., Tsud, N., and Johánek, V., *Prog. Surf. Sci*. **67**, 167 (2001).
19. Tsud, N., Johánek, V., Stará, I., Veltruská, K., Matolín, V., *Thin Solid Films* **391**, 204 (2001).
20. Jeon, Y., Chen, J., Croft, M., *Phys. Rev. B: Condens. Matter* **50**, 6555 (1994).
21. Johánek, V., Tsud, N., Matolín, V., and Stará, I., *Vacuum* **63**, 15 (2001).
22. Šarapatka, T. J., *J. Phys. Chem.* **97**, 11247 (1993).
23. Šarapatka, T. J., *Thin Solid. Films* **226**, 219 (1993).
24. Ealet, B., and Gillet, E., *Surf. Sci.* **281**, 91 (1993).
25. Ealet, B., and Gillet, E., *Surf. Sci.* **367**, 221 (1996).
26. Ogawa, S., and Ichikawa, S., *Phys. Rev. B: Condens. Matter* **51**, 17231 (1995).
27. Tsud, N., Johánek, V., Stará, I., Veltruská, K., and Matolín, V., *Surf. Sci.* **467**, 169 (2000).
28. Matolín, V., Mašek, K., Moreau, O., and Nehasil, V., *Czech. J. Phys.* **47**, 261 (1997).
29. Tougaard S., *J. Vac. Sci. Technol. A* **14**(3), 1415 (1996).
30. Ahn, J., and Rabalais, J. W., *Surf. Sci.* **388**, 121 (1997).
31. *Bull. Alloy Phase Diagrams* **7**(4), (1986).
32. Ealet, B., Elyakhloufi, M. H., Gillet, E., and Ricci, M., *Thin Solid. Films* **250**, 92 (1994).
33. Bordier, G., and Noguera, C., *Phys. Rev. B: Condens. Matter* **44**, 6361 (1991).
34. Hillebrecht, F. U., Fuggle, J. C., Bennett, P. A., Zolnierek, Z., and Freiburg, C., *Phys. Rev. B: Condens. Matter* **27**, 2179 (1983).
35. Matolin, V., Johánek, V., Stará, I., Tsud, N., and Veltruská, K., *J. Electron Spectrosc. Relat. Phenom.* **114–116**, 327 (2001).